Supporting Information for

Achieving enhanced NIR light-induced toxicity via novel hybrid magnetic nanoparticles

Bingxue Qi,[ab] Qi Li,[c] and Lining Miao*[a]

[a] *Department of Nephrology, the Second Hospital of Jilin University, Changchun, China*

[b] *Department of Endocrinology, Jilin Province People's Hospital, Changchun, China*

[c] *Department of Nephrology, the Central Hospital of Jilin City, Jilin, China*

E-mail: miaoliningjlu@163.com

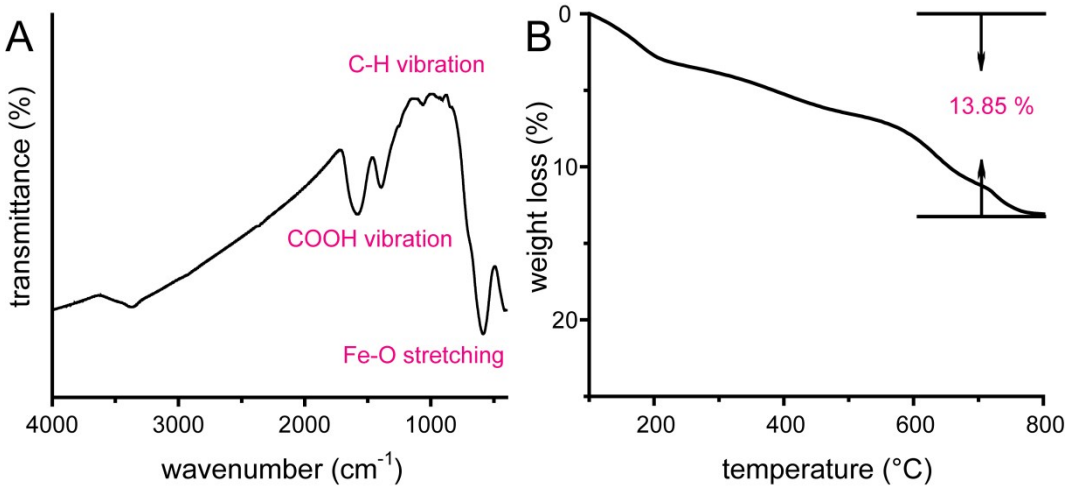

Figure S1. FT-IR spectrum (A) and thermogravimetric analysis curve (B) of Zn^{2+}-doped magnetic nanoparticles.

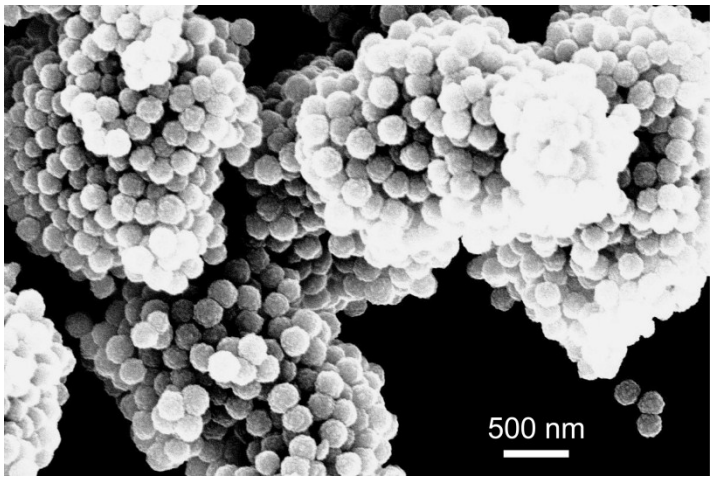

Figure S2. SEM image of Zn^{2+}-doped magnetic nanoparticles prepared without the addition of PEG molecules.

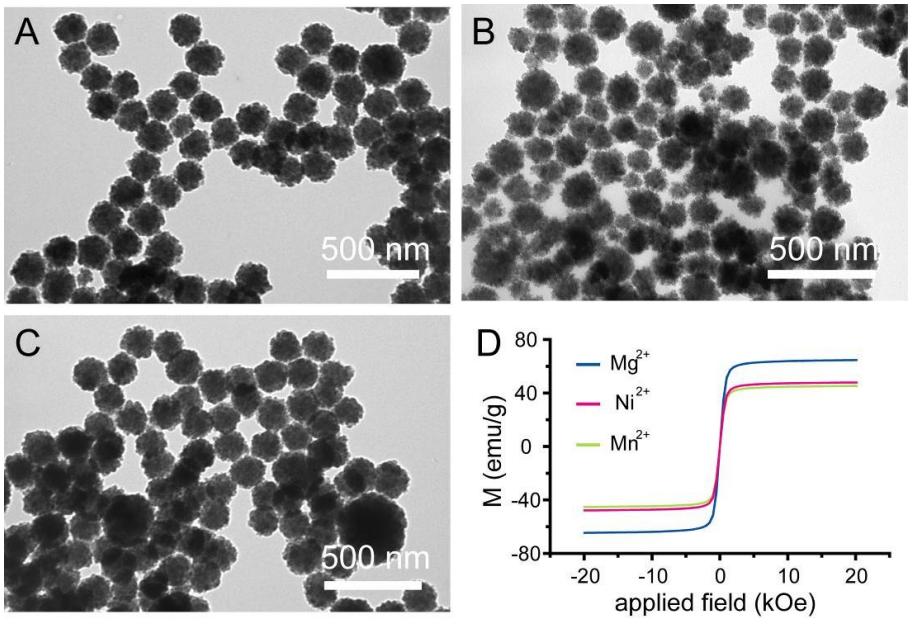

Figure S3. TEM images of Mg^{2+}- (A), Mn^{2+}- (B), and Ni^{2+}-doped magnetic nanoparticles (C). Room temperature magnetic hysteresis loops of above samples (D).

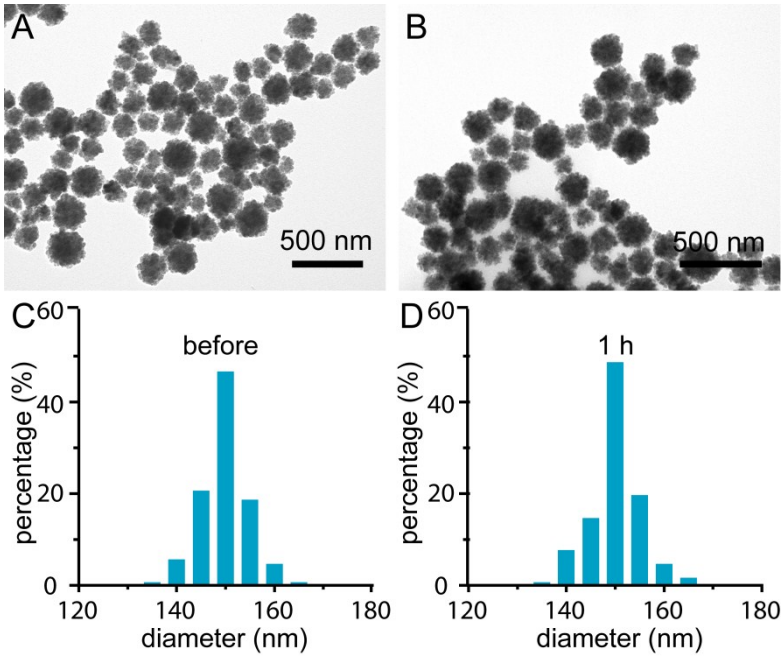

Figure S4. TEM image of Zn^{2+}-doped magnetic nanoparticles after irradiation at 2 W/cm^2 for 0.5 h (A) and 1 h (B). Size distribution of Zn^{2+}-doped magnetic nanoparticles before (C) and 1 h after irradiation at 2 W/cm^2 (D) based on TEM analysis.

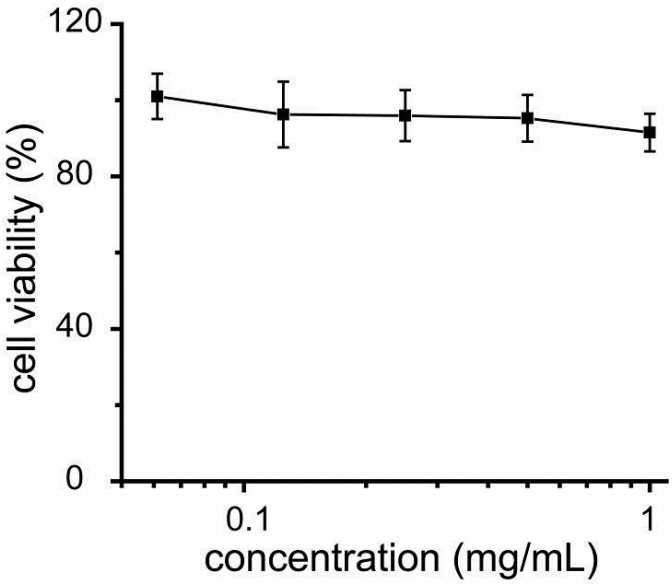

Figure S5. Concentration-dependent viabilities of 786-O cells incubated with Zn^{2+}-doped magnetic nanoparticles.

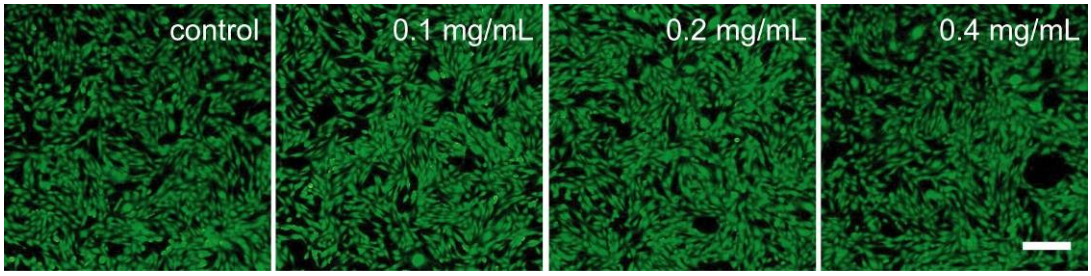

Figure S6. Fluorescence images of calcein AM/PI dual-stained 786-O cells 24 h after co-incubation with Zn^{2+}-doped magnetic nanoparticles. The scale bar is 100 μm.

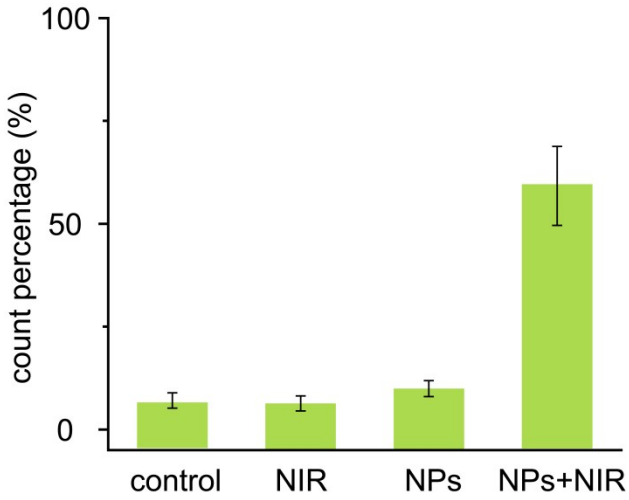

Figure S7. Flow cytometry analysis of ROS generation upon different treatments based on three independent experiments.

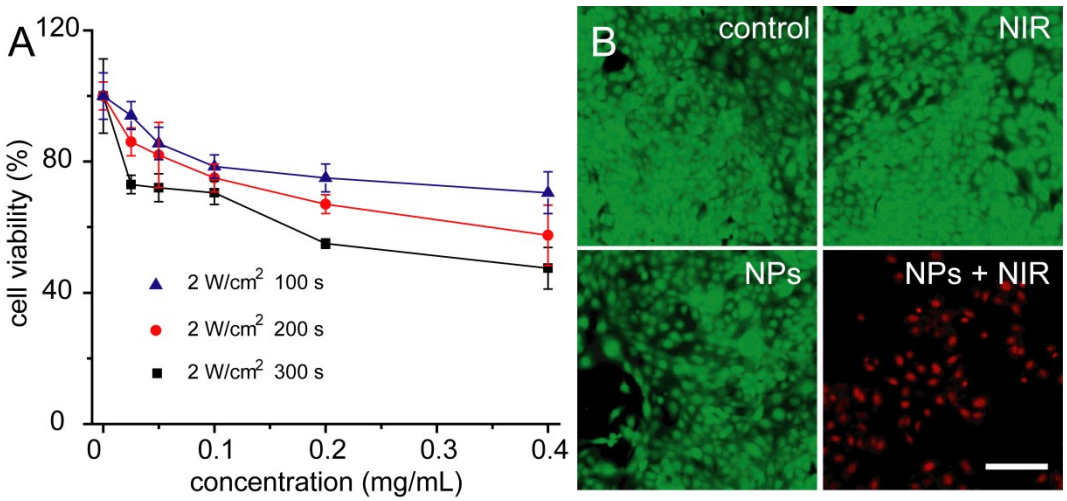

Figure S8. Viabilities of 4T1 cells incubated with Zn^{2+}-doped magnetic nanoparticles treated with a NIR light irradiation (A). Fluorescence images of calcein AM/PI dual-stained 4T1 cells 24 h after incubation with Zn^{2+}-doped magnetic nanoparticles (B). The scale bar is 100 μm.

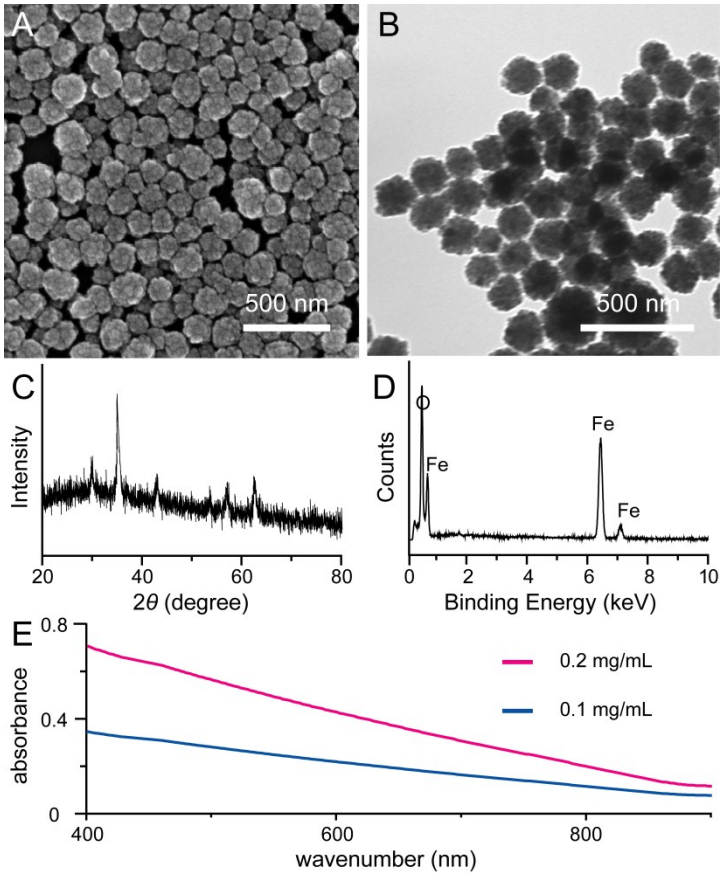

Figure S9. SEM image (A), TEM image (B), wide-angle XRD pattern (C), EDS spectrum (D), and UV-vis spectra (E) of pure Fe_3O_4 nanoparticles prepared with a similar route.

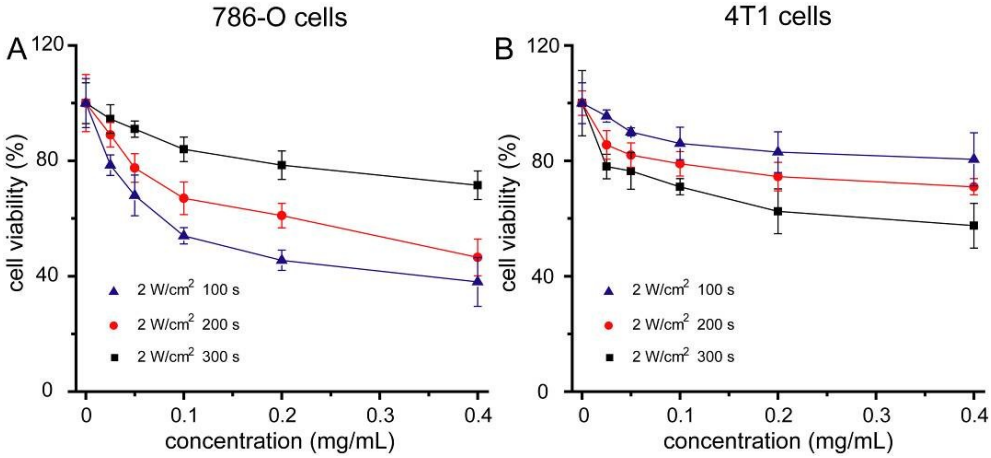

Figure S10. Viabilities of 786-O cells (A) and 4T1 cells (B) incubated with pure Fe_3O_4 nanoparticles prepared with a similar route.

Table S1. Chemical compositions, average sizes, and saturation magnetization values of various hybrid magnetic nanoparticles.

metal precursor	chemical composition	average size (nm)	saturation magnetization (emu/g)
$ZnCl_2$	$Zn_{0.4}Fe_{0.6}Fe_2O_4$	150 nm	76.1 emu/g
$MgCl_2 \cdot 6H_2O$	$Mg_{0.4}Fe_{0.6}Fe_2O_4$	155 nm	64.7 emu/g
$MnCl_2 \cdot 4H_2O$	$Mn_{0.7}Fe_{0.3}Fe_2O_4$	150 nm	45.3 emu/g
$NiCl_2 \cdot 6H_2O$	$Ni_{0.3}Fe_{0.7}Fe_2O_4$	140 nm	47.8 emu/g
$FeCl_3 \cdot 6H_2O$	pure Fe_3O_4	140 nm	76.8 emu/g